

Improving significance of binary black hole mergers in Advanced LIGO data using deep learning : Confirmation of GW151216

Shreejit Jadhav^{1, a}, Nikhil Mukund^{2, 1, b}, Bhooshan Gadre^{3, 1, c}, Sanjit Mitra^{1, d} and Sheelu Abraham^{1, e}

¹Inter-University Centre for Astronomy and Astrophysics (IUCAA), Post Bag 4, Ganeshkhind, Pune 411 007, India

²Max-Planck-Institut für Gravitationsphysik (Albert-Einstein-Institut) and Institut für Gravitationsphysik, Leibniz Universität Hannover, Callinstraße 38, 30167 Hannover, Germany

³Max Planck Institute for Gravitational Physics (Albert Einstein Institute), Am Mühlenberg 1, D-14476 Potsdam-Golm, Germany
(Dated: October 23, 2020)

We present a novel Machine Learning (ML) based strategy to search for compact binary coalescences (CBCs) in data from ground-based gravitational wave (GW) observatories. *This is the first ML-based search that not only recovers all the binary black hole mergers in the first GW transients catalog (GWTC-1), but also makes a clean detection of GW151216*, which was not significant enough to be included in the catalogue. Moreover, we achieve this by *only adding a new coincident ranking statistic (MLStat) to a standard analysis* that was used for GWTC-1. In CBC searches, reducing contamination by terrestrial and instrumental transients, which create a loud noise background by triggering numerous false alarms, is crucial to improving the sensitivity for detecting true events. The sheer volume of data and large number of expected detections also prompts the use of ML techniques. We perform transfer learning to train “InceptionV3”, a pre-trained deep neural network, along with curriculum learning to distinguish GW signals from noisy events by analysing their continuous wavelet transform (CWT) maps. MLStat incorporates information from this ML classifier into the standard coincident search likelihood used by the conventional search. This leads to at least an order of magnitude improvement in the inverse false-alarm-rate (IFAR) for the previously “low significance” events GW151012, GW170729 and GW151216. The confidence in detection of GW151216 is further strengthened by performing its parameter estimation using SEOBNRv4HM_ROM. Considering the impressive ability of the statistic to distinguish signals from glitches, the list of marginal events from MLStat could be quite reliable for astrophysical population studies and further follow-up. This work demonstrates the immense potential and readiness of MLStat for finding new sources in current data and the possibility of its adaptation in similar searches.

INTRODUCTION

The Advanced LIGO [1, 2] and the Advanced Virgo [3] observatories reported the detection of ten binary black-hole mergers [4–9] and a binary neutron star merger [10] in their data spanning the first two observational runs. LIGO and Virgo operating with an improved sensitivity [11] in their third observational run have detected tens of gravitational-wave (GW) candidates [12] including a binary black hole (BBH) merger with asymmetric masses and a possible heavy binary neutron star merger [13–16] and tens of more triggers were publicly announced as potential events. As the LIGO and Virgo detectors advance their sensitivities and with KAGRA joining the search [17, 18], the rate of GW detections is expected to increase multi-fold [19].

Currently, these detectors make use of both modelled and unmodelled searches to detect potential GW signals in their calibrated data [20–24]. Had the noise in the detectors been Gaussian and stationary, only the time-coincidence of GW signals in more than one detectors would be a decisive criterion to find a candidate event. The quadrature sum of signal-to-noise ratios (SNRs) in individual detectors would suffice as the ranking statistic [25–28] and it would have been possible to model the background analytically in this simplistic case [29, 30]. However, the data is heavily contaminated by non-stationary and non-Gaussian transients of instrumental and terrestrial origin, also known as ‘glitches’. These noise transients mimic astrophysical signals by bypassing the search pipelines and result in a persistent problem of false

alarms [31, 32] which impact the search sensitivity of coalescing compact binaries and GW bursts. As the detectors become more sensitive, along with an improvement in detection rate of GW signals the rate of occurrence of such glitches may also increase, resulting in a considerable number of real GW candidates being reported with reduced significance.

Various methods of compact binary coalescence (CBC) search [20, 22, 33] were used to detect gravitational wave sources in LIGO’s first observational run (O1) [34, 35]. These searches resulted in two confident BBH detections viz., GW150914 and GW151226 at false-alarm rate (FAR) $< 6.0 \times 10^{-7} \text{ yr}^{-1}$ ($> 5.3\sigma$) each and a third detection viz. GW151012 with a higher FAR of 0.37 yr^{-1} (1.7σ) [4, 36, 37]. Later, using an improved search method, the FAR of GW151012 could be reduced to 0.17 yr^{-1} [9]. Similarly, in the offline PyCBC analysis of the second observational run (O2), GW170729 was detected with a FAR of 1.36 yr^{-1} . The statistic used in 2-OGC [38] reduced the FAR values of GW151012 and GW170729 to 0.0045 and 0.15 respectively. An investigation shows that the triggers with $\text{SNR} \approx 9$ mainly consist of false alarms caused by glitches [37], which increase the noise background and reduce the significance of marginal events, thereby obstructing the science we can do with them.

In recent years, machine learning has been extensively applied to GW data analysis [39–46]. In this work we demonstrate how application of a machine learning algorithm, designed to discern real events from spurious glitches, can be used to improve the standard matched filtering based analysis used by LIGO [9]. We use transfer learning with Incep-

tionV3 [47] – an image-based deep learning classifier pre-trained on over a million images of day-to-day objects – and retrain it to classify CBCs and glitches in the LIGO data. The classifier gives a probability of a trigger belonging to the ‘CBC’ class among a number of transient classes, which we use to modify the ranking statistic and construct the new statistic (*MLStat*). Here we extend the PYCBC search analysis used in GWTC-1 [9, 48], however, a similar methodology can also be implemented with other pipelines like cWB [22], GSTLAL [21] and MBTA [23] to seek sensitivity improvements. We show significant improvement in the inverse-false-alarm rates (IFARs) of the low-significance events GW151012 and GW170729 with *MLStat*. We also detect the new candidate event GW151216 from O1 [49, 50] and report the parameter estimation results just as a verification.

INCORPORATING MACHINE LEARNING

Success for any ML classifier depends on its ability to learn the relevant features from the dataset and then develop a strategy to optimally separate the different classes by judiciously weighting the different learned parameters. Obtaining an optimal decision boundary in classifiers requires the overlap in the feature-space to be as minimal as possible. Within astronomy community, features are traditionally chosen by a domain expert as in the case of several stellar [51–53], GRB [54], galaxy [55–57], quasar [58–60] and GW classification schemes [61]. The advent of GPUs and the availability of larger training sets have resulted in techniques based on deep learning to gain more prominence in recent years. Convolutional neural networks (CNNs), in particular, have shown remarkable success in tasks pertaining to image classification and are consistently outperforming feature-based classical ML techniques when applied to standard bench-marking datasets [62, 63].

Large architectures of CNNs, like Google’s Inception model and Microsoft’s Resnet model, have been trained using cutting-edge GPU technology on large datasets containing images of objects in day-to-day life [47, 64]. Transfer learning makes use of the rich feature extraction capability of such pre-trained models and allows repurposing them for a different classification task. The final few layers of a pre-trained network are replaced with trainable new layers while the rest of the network architecture is retained as before. The training of such a network on a new image dataset essentially maps the extracted features to new classes, thus making the training faster while still maintaining the accuracy. Another advantage of transfer learning is that the amount of training data required to reach the prescribed accuracy is hugely reduced.

Inception networks [65] put forward a strategy for making effective deeper networks through tactics different from merely increasing either the layers or neurons per layer. For example, the InceptionV3 network [47] differs from the traditional monolithic CNN architecture through the usage of factorizing convolutions, parallel structures, and extensive di-

mensionality reduction techniques. These schemes make the architecture well suited for applications with stringent memory and computational constraints but still provide state-of-the-art performance without over-fitting the data.

The transients of astrophysical or terrestrial origin seen in LIGO data have a peculiar evolution in the time-frequency domain. This provides a 2D representation that can be analysed by the image-based classifiers mentioned above. During the early inspiral phase of a CBC waveform, Einstein’s quadrupole formula for gravitational wave luminosity can be solved with a non-relativistic approximation to obtain the evolution of frequency with time as $f \propto (t_c - t)^{-3/8}$, where t_c is the time of coalescence [66]. This explains the peculiar chirp-like shape of CBC signals in time-frequency maps which can be exploited to differentiate them from glitches. We get much more accurate description of the full time-frequency evolution of CBCs using the Inspiral-Merger-Ringdown (IMR) waveforms. As compared to the χ^2 weighing [67] which compares the template and data only in frequency bins, by analysing the trigger morphology in time-frequency maps, we are, in a way, comparing the power distribution of the transient in both time and frequency bins.

Previously, Omega scans have been used to map the LIGO data to the time-frequency domain where the chirp-like evolution of CBCs can be distinguished from other noise transients more effectively [61, 68]. We use the continuous wavelet transform (CWT) with an analytic Morlet (*amor*) wavelet to construct time-frequency scalograms of the whitened strain data to be analysed. Wavelets, in general, provide a much better time and frequency resolution compared to short-time Fourier transform (STFT) [69]. Discriminator based on relative wavelet energy has previously been demonstrated to be effective in separating various transient classes and was successfully applied to Advanced LIGO’s first observational run data [61]. We create CWT scalograms by whitening and band-passing the data around a GPS trigger between 16Hz and 512Hz. We consider a data slice of 1 second duration with the trigger time kept at centre, convert it into a scalogram and save it as a grayscale image with pixels denoting absolute values of CWT coefficients. As InceptionV3 is trained on natural images, the features extracted from different channels are most likely to differ from each other based on the biases in the images of natural objects. The choice of using grayscale colormap ensures the complete glitch morphology is saved in each of the three channels rather than getting divided based on the colormap. The network’s convolution filters then observe the full evolution of a transient in each channel, and the channel-based biases are marginalised.

The CWT image data for training was generated by using a manually curated subset of GravitySpy data [68, 70]. As transfer learning involves training a significantly fewer number of neurons, typically, a very small amount of training data (a few hundred images per class) suffices. This size also makes manual curation practically possible. Due to band passing, classes like 1080Lines, 1400Ripples and Violin-Mode were rendered redundant and were thus excluded. Also, the

Time Class	AC	BL	EL	GN	HX	CBC	LM	LFB	LFL	PL1	PL2	RBL	SL	SC	TM	WL	WH
AC	92.5	0.0	0.0	0.0	0.0	2.5	0.0	0.0	0.0	2.5	0.0	0.0	0.0	2.5	0.0	0.0	0.0
BL	0.0	87.2	0.0	0.0	0.5	0.0	2.1	0.0	0.0	0.0	0.0	0.0	8.0	0.0	0.0	0.0	2.1
EL	0.0	0.0	100.0	0.0	0.0	0.0	0.0	0.0	0.0	0.0	0.0	0.0	0.0	0.0	0.0	0.0	0.0
GN	0.0	0.0	0.0	95.5	0.0	4.5	0.0	0.0	0.0	0.0	0.0	0.0	0.0	0.0	0.0	0.0	0.0
HX	0.0	0.0	0.0	0.0	100.0	0.0	0.0	0.0	0.0	0.0	0.0	0.0	0.0	0.0	0.0	0.0	0.0
CBC	0.0	0.0	0.0	3.0	0.0	97.0	0.0	0.0	0.0	0.0	0.0	0.0	0.0	0.0	0.0	0.0	0.0
LM	0.0	0.7	0.0	0.0	0.7	0.0	97.8	0.0	0.0	0.0	0.0	0.0	0.7	0.0	0.0	0.0	0.0
LFB	0.0	0.0	0.0	1.6	0.0	1.6	92.2	3.1	0.0	0.0	0.0	0.0	0.0	0.0	1.6	0.0	0.0
LFL	0.0	0.0	0.0	0.0	0.0	0.0	2.8	91.5	0.0	1.4	0.0	1.4	0.0	0.0	0.0	2.8	0.0
PL1	1.0	0.0	0.0	0.0	0.0	0.0	0.0	0.0	0.0	99.0	0.0	0.0	0.0	0.0	0.0	0.0	0.0
PL2	7.5	0.0	0.0	0.0	0.0	0.0	0.0	0.0	2.5	90.0	0.0	0.0	0.0	0.0	0.0	0.0	0.0
RBL	0.0	3.5	0.7	0.0	0.0	0.7	0.0	0.0	0.0	0.0	0.0	92.9	0.0	0.7	0.0	0.0	1.4
SL	4.3	0.0	0.0	0.0	0.0	0.0	0.0	0.0	0.0	0.0	0.0	0.0	6.9	94.8	0.0	0.0	0.0
SC	0.0	0.0	0.0	0.0	0.0	0.0	0.0	0.0	0.0	0.0	0.6	0.0	0.0	99.4	0.0	0.0	0.0
TM	0.6	0.6	0.0	0.0	0.0	0.0	0.0	0.0	0.0	0.0	0.0	1.3	0.0	0.0	97.4	0.0	0.0
WL	0.0	0.0	0.0	0.0	0.0	0.0	10.0	0.0	0.0	10.0	0.0	0.0	0.0	0.0	0.0	90.0	0.0
WH	0.0	1.8	0.0	0.0	0.0	1.8	0.0	0.0	0.0	2.8	0.0	0.9	0.0	0.0	0.0	92.7	0.0
	AC	BL	EL	GN	HX	CBC	LM	LFB	LFL	PL1	PL2	RBL	SL	SC	TM	WL	WH

FIG. 1. Confusion matrix (in percent) for the combined validation data from all the levels of curriculum learning. A total of 17 transient classes have been used, viz., Air Compressor (AC), Blip (BL), Extremely Loud (EL), Gaussian Noise (GN), Helix (HX), Injected Chirp (CBC), Light Modulation (LM), Low Frequency Burst (LFB), Low Frequency Lines (LFL), Power Line (PL1), Power Line2 (PL2), Repeating Blips (RBL), Scattered Light (SL), Scratchy (SC), Tomte (TM), Wandering Line (WL) and Whistle (WH). The performance of CBC class is of particular importance as it directly affects MLStat.

Power-Line class was divided into Power-Line and Power-Line2 to separate shorter and longer transients. Data for CBC class was generated by considering real LIGO strain data and by injecting CBC signals with SNR values in the range (4, 20) with IMRPhenomD waveform approximant. The component masses were sampled between ($5M_{\odot}$, $95M_{\odot}$) with a constraint on total mass, $M \leq 100M_{\odot}$. Besides, a separate class named Gaussian-Noise was created, which consisted of plain whitened strain data picked from the same time durations of LIGO data that did not contain glitches. Certain glitch classes were omitted from the data due to lack of feature distinction in CWT maps. The final list of transient classes can be found in Fig. 1.

To perform transfer learning, we load the 316 layers deep directed acyclic graph (DAG) network of *InceptionV3* and freeze the weights of the first 250 layers. We also add a 40% *Dropout* layer and an additional *Fully Connected* layer of size 1024 with *Leaky-ReLu* activation function before the final replaced *Fully Connected* layer which now maps to the 17 transient classes with *Softmax* activation function. We adopt a curriculum learning strategy specifically in CBC class to train the network step-by-step, going from higher SNR values to lower ones. We observed that this method remarkably increased the network accuracy as compared to a single training session with full data. The network was trained using stochastic gradient descent with momentum (SGD-M) [71]. After three training levels, the trained network achieves a training accuracy of 99.2% and a validation accuracy of 94.2%. Fig. 1 shows the confusion matrix for the validation data across all three levels.

For each evaluated image, the network outputs a posterior probability across the 17 transient classes. However, only the

probability corresponding to CBC class (P_{CBC}) will be used in our analysis. To further validate the performance of P_{CBC} with independent test data, we generated 5000 new samples of CBC and Gaussian-Noise from real LIGO data. With a P_{CBC} threshold of 0.9, it was found that more than 91.2% of the injections with $\text{SNR} > 7$ were identified by the classifier. Though this fraction starts deteriorating below $\text{SNR} 7$, significance of the events detected with high P_{CBC} values in this region will improve by a large margin. Against Gaussian-Noise the P_{CBC} distribution was found to peak near zero and more than 95% samples were detected with $P_{\text{CBC}} < 0.2$. Also, from the analysed O1 and O2 data, it was seen that majority of the triggers were classified with very low P_{CBC} values. The small fraction of triggers with high P_{CBC} values are very unlikely to be coincident in both the detectors as demanded by the MLStat construction explained in the next section.

CONSTRUCTION OF MLSTAT

PyCBC workflow performs matched filtering on the data with a bank of templates. Triggers are then collected by thresholding and clustering the SNR time series. The SNR is re-weighted with two types of noise suppressing vetoes and a semi-coherent ranking statistic (we call it base statistic hereafter) ensuring approximately trigger rate estimation across the search parameter space to determine the significance of events [48, 67, 72]. We analyse the triggers with our classifier and build the ML tool as an augmentation of the standard pipeline used by LIGO.

As mentioned in the previous section, for each trigger, our classifier gives the probability (P_{CBC}) of it belonging to the CBC class. Thus, the parameter space used for the construction of the new statistic, MLStat, extends to $\Theta' = (\Theta, P_{\text{H}}^{\text{CBC}}, P_{\text{L}}^{\text{CBC}})$, where Θ is the parameter space considered by the base statistic $\tilde{\rho}$. Here, H/L in the subscripts denote Hanford/Livingston observatories respectively. The original likelihood ratio for detection of gravitational wave signal is given by,

$$\Lambda(H_{\lambda}|s) = \frac{p(s|H_{\lambda})}{p(s|H_0)}$$

where, $s(t)$ is the time series strain data, H_{λ} is the hypothesis stating that the signal $h(t, \lambda)$ is present in $s(t)$ and H_0 is the null hypothesis. We update the above likelihood ratio to include P_{CBC} as follows,

$$\Lambda'(H_{\lambda}|s) = \frac{p(s|H_{\lambda}) * P_{\text{H}}^{\text{CBC}} * P_{\text{L}}^{\text{CBC}}}{p(s|H_0)}. \quad (1)$$

This results in a new coincident ranking statistic (MLStat) $\tilde{\rho}_{\text{ml}}$, a simple extension to the base coincident statistic $\tilde{\rho}_{\text{c}}$,

$$\tilde{\rho}_{\text{ml}}^2 = \tilde{\rho}_{\text{c}}^2 + 2 * \log(P_{\text{combined}}^{\text{CBC}}), \quad (2)$$

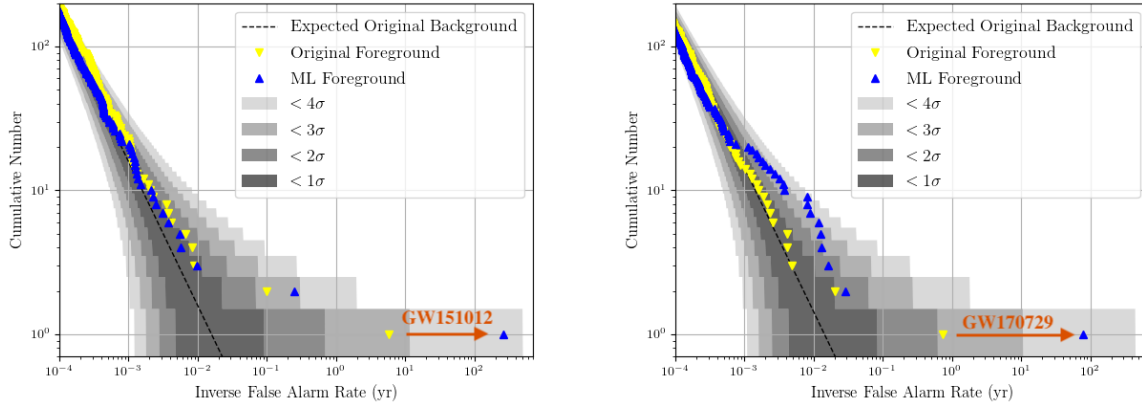


FIG. 2. Significance improvement for GW151012 (left) and GW170729 (right): Cumulative histograms of foreground events in base statistic (yellow) and MLStat (blue) and the expected background plotted against the inverse false-alarm rate. Shaded regions show the sigma intervals for Poisson uncertainty. The loudness of first ~ 20 foreground events with MLStat in O2 is not a systematic bias and is rather an effect of the low number statistics which has been observed with other statistics before (See Fig. 2 and Fig. 3 in [9]). With MLStat, IFAR value of the most significant foreground event GW151012 (GW170729) improves from 5.84 (0.73) to 258 (79.3). We also observed that the event sequence according to IFAR values was considerably shuffled in MLStat. The second most significant event viz., 151016, in O1 chunk has IFAR 0.25.

where $P_{\text{combined}}^{\text{CBC}} = P_{\text{H}}^{\text{CBC}} * P_{\text{L}}^{\text{CBC}}$. This implies that for detection by this statistic, a signal should look CBC-like in both the detectors within the light travel time window.¹

The real CBC signals should have P_{CBC} values close to 1, thus making the second term in Eq. 2 very small. The MLStat values will be very close to the base statistic for such events. On the other hand, noise triggers in the background which do not have a CBC-like composition in CWT maps will be pushed to lower values. Thus, discriminating real events from the noise contamination results in a decreased background, which effectively improves the significance of true CBC events.

ANALYSIS OF O1 AND O2 DATA

We re-purpose the offline analysis data of PYCBC search described in GWTC-1 [9, 74]. We analysed two chunks of data from O1 and O2 that contained the low significance events GW151012 and GW170729 respectively. The analysis consisted of ~ 5.9 days of coincident data during October 8-20, 2015 for O1 and ~ 5.3 days of coincident data starting from July 27 to Aug 5, 2017 for O2.

CWT maps of duration 1 second were created keeping the PYCBC triggers in the centre. These images were then analysed with the ML classifier to get the respective P_{CBC} values. We observed that the classifier is immune to changes in

CWT maps corresponding to small translations in time, thus allowing us to round off the trigger GPS times to one decimal place. Analyses of multiple triggers lying within a time window of 0.1 second is thus avoided. The P_{CBC} values were recorded for all the triggers from both the detectors. The coincident MLStat is then calculated using Eq. 2 with PYCBC GWTC-1 statistic as the base statistic. The improvement in significance of GW151012 and GW170729 with MLStat is shown in Fig. 2. The IFAR of GW151012 (GW170729) increases from 5.84 (0.73) in base statistic to 258 (79.3) in MLStat, thus making them very confident detections.

Extension of the analysis

Though doing a full analysis of any of the observational runs is beyond the scope of the current work, we wish to get an estimate of what we should expect from the extended analysis. We make an assumption that the improvement in the background estimation is similar across all the chunks in the observational run. We then note the improvement in the significance of the full set of foreground triggers against the analysed chunk of that run and estimate their improved IFAR values with respect to the background of the original chunks they belonged to. Calculating these MLStat IFAR values of full O1 and O2 foregrounds, we confirm the detection of one event in O1, viz. GW151216, that has been discussed in the literature before [38, 49, 50, 75–77], whose IFAR improved from 0.00173 years in GWTC-1 to 1.983 years with MLStat. CWT maps of the events that become significant with our analysis are shown in Fig. 3.

We list the combined foreground of O1 and O2 with $\text{FAR}_{\text{ml}} < 1$ per month in Table I. GW170818 was not de-

¹ Note that we do not use P_{CBC} for fitting the single detector event rate as done in the base GWTC-1 statistic which may give us further improvements, especially in the regions of the parameter space which can suffer due to high false-alarm rates and thus show reduced sensitivity.

TABLE I. List of candidate events from the extended analysis of O1 and O2 sorted by FAR_{ml} [73]. All the catalogue events [9] are successfully found by our analysis. Exceptions are GW170817 (excluded from the analysis) and GW170818 (not found by PYCBC). Five marginal events with $\text{FAR}_{\text{ml}} < 1/\text{month}$ are reported, which may be worth following-up and may prove to be useful for estimating astrophysical distributions. Mass and spin values (detector frame) are those of the best matching search template giving highest coincident MLStat and need not match the full Bayesian parameter estimation results. We report one to two orders of magnitude improvements in IFAR for GW151012 and GW170729, obtained by analysing the respective data chunks which makes them definite confident detections. The FAR_{ml} quoted for rest of the events are inferred by assuming similar significance improvements across respective observational runs. FAR_{base} values are also given for comparison. The newly detected event GW151216 is shown in bold.

UTC	MLStat	FAR_{base} [yr^{-1}]	FAR_{ml} [yr^{-1}]	m_1^t [M_\odot]	m_2^t [M_\odot]	s_{2z}^t	s_{1z}^t	P_H^{CBC}	P_L^{CBC}
2017-08-14T10:30:43 ^a	12.7	$< 1.3 \times 10^{-5}$	$< 1.3 \times 10^{-5}$	33.14	25.38	0.68	-0.95	0.999	0.999
2017-01-04T10:11:58 ^a	10.8	$< 1.4 \times 10^{-5}$	$< 1.4 \times 10^{-5}$	40.87	13.91	-0.70	0.80	0.996	0.999
2015-09-14T09:50:45 ^a	15.5	$< 1.5 \times 10^{-5}$	$< 1.5 \times 10^{-5}$	44.21	32.16	0.78	-0.86	0.999	0.999
2015-12-26T03:38:53 ^a	11.7	$< 1.7 \times 10^{-5}$	$< 1.7 \times 10^{-5}$	14.83	8.50	-0.09	0.81	0.873	0.611
2017-08-23T13:13:58 ^a	10.2	$< 3.3 \times 10^{-5}$	$< 3.3 \times 10^{-5}$	47.94	16.22	-0.92	0.64	0.998	0.999
2017-08-09T08:28:21 ^a	10.5	$< 1.45 \times 10^{-4}$	$< 1.45 \times 10^{-4}$	47.62	16.21	-0.57	0.90	0.627	0.999
2017-06-08T02:01:16 ^a	12.7	$< 3.1 \times 10^{-4}$	$< 3.1 \times 10^{-4}$	16.82	6.10	0.11	0.88	0.996	0.999
2015-10-12T09:54:43 ^{a,d}	9.0	0.17	3.87×10^{-3}	25.75	17.60	-0.36	0.73	0.838	0.994
2017-07-29T18:56:29 ^{a,d}	8.7	1.36	1.26×10^{-2}	67.52	32.53	0.27	-0.09	0.988	0.998
2015-12-16T09:24:16^b	8.2	57.74	0.5043	41.78	34.35	0.85	0.98	0.793	0.996
2015-10-16T13:57:41 ^{c,d}	8.0	–	3.96	364.00	5.35	0.98	-0.24	0.995	0.745
2017-07-23T12:45:56	7.8	273.19	5.76	33.26	11.22	-0.42	-0.62	0.236	0.882
2015-11-02T06:46:59	7.9	1049.95	7.96	224.16	2.77	0.99	0.43	0.747	0.999
2015-11-28T20:20:29	7.8	1078.63	8.64	51.93	1.57	0.42	0.02	0.759	0.863
2017-04-12T01:49:51	7.8	1355.84	11.26	46.04	1.19	0.23	0.03	0.973	0.670

^a GWTC-1 events; ^b Not present in GWTC-1; ^c Not present in the PYCBC analysis used in GWTC-1;

^d Definite FAR_{ml} (obtained from analysed chunks)

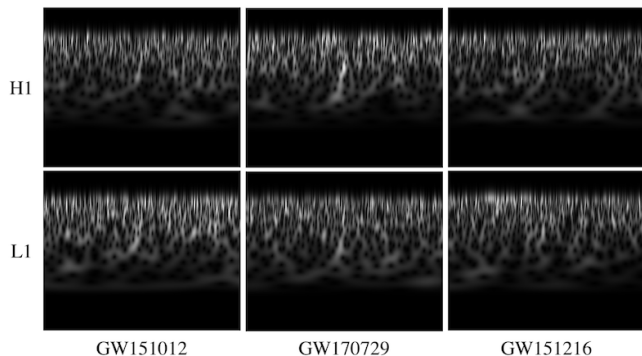


FIG. 3. CWT maps of events that gain significance with MLStat. Whitened strain data of duration one second, band-passed between 16Hz and 512Hz, is used to generate the Gray-scale images that are fed to the classifier.

ected by PYCBC and thus does not show up in our analysis. Also, GW170817 has been excluded from the analysis as it falls out of the parameter space used for training the classifier and the CBC-tracks for such long duration signals may

not be visible in the CWT map. We intend to build a more comprehensive ML tool covering larger parameter space in the followup work.

We report the parameter estimation results for GW151216 using the fully Bayesian code BILBY [78, 79]. For the analysis, we estimate the noise power spectral density with BAYESWAVE [80] using 16 sec of data around GW151216. The posteriors with SEOBNRV4HM_ROM model [81] which includes higher order modes, are shown in the Fig. 4 for some of the parameters. There are other detailed analyses for the event which take in to account other various waveform models and priors can be found in [75–77]. We find that GW151216 has component masses of $46.8_{-17.7}^{+12.5} M_\odot$ and $23.6_{-9.6}^{+5.6} M_\odot$ with the inverse mass ratio of ~ 2 with the luminosity distance of $2269_{-1033}^{+1193} \text{Mpc}$. Also 90% credible intervals for effective inspiral spin parameter show non-zero spins with χ_{eff} of $0.56_{-0.5}^{+0.23}$. The expected posteriors from the parameter estimation also serves as a check that the event is indeed BBH merger. We also plan to analyse the other marginal events in detail with data quality checks and parameter estimation.

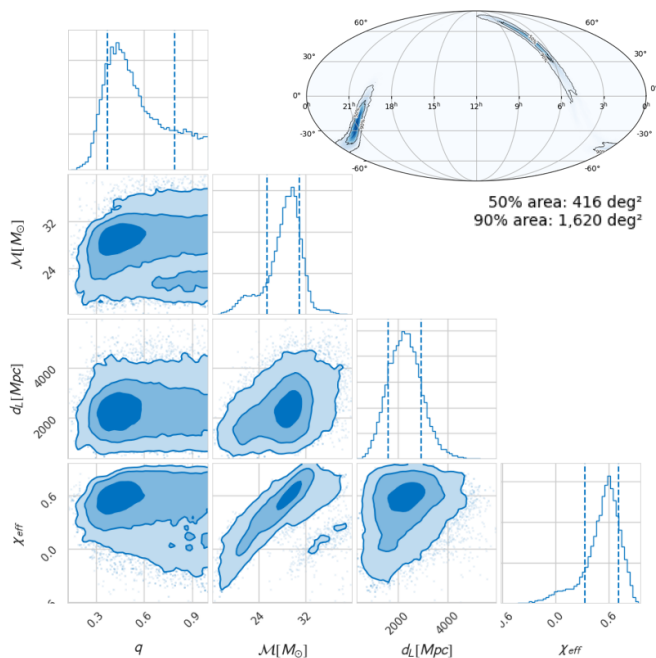


FIG. 4. Bayesian parameter estimation posteriors for the event GW151216 using SEOBNRV4HM_ROM waveform model. We can clearly see the evidence for unequal masses with component masses of $46.8^{+12.5}_{-17.7} M_{\odot}$ and $23.6^{+5.6}_{-9.6} M_{\odot}$ and non-zero spin with χ_{eff} of $0.56^{+0.23}_{-0.5}$ and luminosity distance of 2269^{+1193}_{-1033} Mpc. The corresponding sky localisation map is also overlaid.

CONCLUSIONS

As the sensitivities of ground-based GW interferometers improve, the rate of detection of astrophysical events is going to increase, posing a challenge to the analyses to cope up with the large number of events. The major hurdle in this task arises from the terrestrial and instrumental glitches, and their occurrence may increase with sensitivity. This issue may become even more severe with time as the density of events observed in the distant universe with statistically lower SNRs is expected to increase. Improving the fraction of true events in the set of potential triggers can significantly reduce this burden. Perhaps in the future ML will also help us in expanding the dimension and volume of the parameter space for astrophysical searches.

In this work, we demonstrated the capability of machine learning to improve the significance of CBC signals and to discard false triggers by integrating it with the existing analysis framework of PYCBC. We used transfer learning with InceptionV3, a pre-trained image based classifier, for effective identification of binary black hole mergers against glitches in LIGO data. We repurpose the PYCBC offline search data to re-analyse the matched filter triggers for two chunks of data from O1 and O2 that contained the events GW151012 and GW170729. We use the retrained InceptionV3 network to classify the continuous wavelet transform maps, a representation of time series data in time-frequency domain, of these

triggers and get the P_{CBC} values which are used to construct a new ranking statistic MLStat – a simple extension of the conventional coincident statistic. This helped in breaking the degeneracy between the real CBC signals and the noise transients that pass the conventional analysis and result in an increased background. With MLStat, we achieve a considerable reduction in background and an improved separation of foreground. We report one to two orders of magnitude reduction in false alarm rates for the low significance events GW151012 and GW170729 with MLStat as compared to the statistic used by PYCBC in the first GW transient catalog (GWTC-1).

This is the first time a machine learning based search algorithm was able to detect all the binary black hole mergers in GWTC-1 with same or better significance. By assuming similar improvements in the false alarm rates across the observational run, as seen in the respective analysed chunks, we also confirm the detection of the event GW151216, which was not included in GWTC-1 lists of confirmed and marginal events due to lack of significance. While the existence and nature of this event is debated [38, 50, 75–77], to boost confidence in this detection and for demonstration of completeness of the process of a new detection using MLStat, we perform parameter estimation for this event with an improved waveform model with higher order modes SEOBNRV4HM_ROM [81]. Considering the ability of our method to distinguish the false triggers from astrophysical events, the list of sub-threshold events reported with MLStat may be more reliable for astrophysics (e.g., population studies) but further follow-up though a data quality check would still be required.

That, by tuning a generic ML algorithm and introducing a simple extension to the ranking statistic, we could achieve these major milestones, shows the enormous potential in ML, provided we can adapt it with fine understanding of the problem in hand. There is ample scope to improve our present analysis and, in general, several avenues may be explored to introduce machine learning based algorithms in GW analyses.

ACKNOWLEDGMENTS

Authors express thanks to Ninan Sajeeth Philip, Shivaraj Kandhasamy and the LIGO-Virgo-KAGRA Collaboration for their valuable comments and suggestions. Some of the results in this work have been derived using the PESUMMARY package [82]. SJ and NM acknowledge Council for Scientific and Industrial Research (CSIR), India, for providing financial support as Senior Research Fellows. NM also expresses thanks to the Max Planck Society and the Leibniz University, Hannover, for providing support as a post-doctoral researcher. BG would like to acknowledge the support of the Max Planck Society as a post-doctoral fellow and the support of University Grants Commission (UGC), India. We acknowledge the use of IUCAA LDG cluster Sarathi and GWA for the computational work. The follow up analysis for GW151216 is performed with the HPC clusters HYPATIA at

the Max Planck Institute for Gravitational Physics, Potsdam-Golm. SM and SA acknowledge support from the Department of Science and Technology (DST), India, provided under the Swarna Jayanti Fellowships scheme. This document has been assigned IUCAA preprint number IUCAA-03/2020 and LIGO document number LIGO-P2000399.

^a shreejit@iucaa.in

^b nikhil.mukund@aei.mpg.de

^c bhooshan.gadre@aei.mpg.de

^d sanjit@iucaa.in

^e sheelu@iucaa.in

- [1] J. Aasi *et al.* (LIGO Scientific Collaboration and Virgo Collaboration), *Classical and Quantum Gravity* **32**, 074001 (2015).
- [2] B. P. Abbott *et al.* (LIGO Scientific Collaboration and Virgo Collaboration), *Phys. Rev. Lett.* **116**, 131103 (2016).
- [3] F. Acernese *et al.*, *Classical and Quantum Gravity* **32**, 024001 (2014).
- [4] B. P. Abbott *et al.* (LIGO Scientific Collaboration and Virgo Collaboration), *Phys. Rev. Lett.* **116**, 061102 (2016).
- [5] B. P. Abbott *et al.* (LIGO Scientific Collaboration and Virgo Collaboration), *Phys. Rev. Lett.* **116**, 241103 (2016).
- [6] B. P. Abbott *et al.* (LIGO Scientific and Virgo Collaboration), *Phys. Rev. Lett.* **118**, 221101 (2017).
- [7] B. P. Abbott *et al.*, *The Astrophysical Journal* **851**, L35 (2017).
- [8] B. P. Abbott *et al.* (LIGO Scientific Collaboration and Virgo Collaboration), *Phys. Rev. Lett.* **119**, 141101 (2017).
- [9] B. P. Abbott *et al.* (LIGO Scientific Collaboration and Virgo Collaboration), *Phys. Rev. X* **9**, 031040 (2019).
- [10] B. P. Abbott *et al.* (LIGO Scientific Collaboration and Virgo Collaboration), *Phys. Rev. Lett.* **119**, 161101 (2017).
- [11] “Observatory Status,” <https://www.ligo.caltech.edu/page/observatory-status>.
- [12] “Gravitational-wave candidate event database,” <https://gracedb.ligo.org/>.
- [13] R. Abbott *et al.* (LIGO Scientific Collaboration and Virgo Collaboration), *Phys. Rev. D* **102**, 043015 (2020).
- [14] B. P. Abbott *et al.*, *The Astrophysical Journal* **892**, L3 (2020).
- [15] R. Abbott *et al.* (LIGO Scientific Collaboration and Virgo Collaboration), *Phys. Rev. Lett.* **125**, 101102 (2020).
- [16] R. Abbott *et al.*, *The Astrophysical Journal* **896**, L44 (2020).
- [17] Y. Aso, Y. Michimura, K. Somiya, M. Ando, O. Miyakawa, *et al.* (The KAGRA Collaboration), *Phys. Rev. D* **88**, 043007 (2013).
- [18] T. Akutsu, M. Ando, K. Arai, Y. Arai, S. Araki, *et al.*, (2020), [arXiv:2005.05574](https://arxiv.org/abs/2005.05574) [physics.ins-det].
- [19] B. P. Abbott *et al.*, *Living Reviews in Relativity* **21**, 3 (2018).
- [20] S. A. Usman, A. H. Nitz, I. W. Harry, C. M. Biwer, D. A. Brown, *et al.*, *Classical and Quantum Gravity* **33**, 215004 (2016).
- [21] S. Sachdev, S. Caudill, H. Fong, R. K. L. Lo, C. Messick, *et al.*, “The gstlal search analysis methods for compact binary mergers in advanced ligo’s second and advanced virgo’s first observing runs,” (2019), [arXiv:1901.08580](https://arxiv.org/abs/1901.08580) [gr-qc].
- [22] S. Klimentenko, G. Vedovato, M. Drago, F. Salemi, V. Tiwari, *et al.*, *Phys. Rev. D* **93**, 042004 (2016).
- [23] T. Adams (LIGO Scientific Collaboration and Virgo Collaboration) (2015) [arXiv:1507.01787](https://arxiv.org/abs/1507.01787) [gr-qc].
- [24] Q. Chu, PhD (2017).
- [25] L. Zubakov and V. Wainstein, “Extraction of signals from noise,” (1962).
- [26] C. Cutler, T. A. Apostolatos, L. Bildsten, L. S. Finn, E. E. Flanagan, *et al.*, *Phys. Rev. Lett.* **70**, 2984 (1993).
- [27] A. Pai, S. Dhurandhar, and S. Bose, *Phys. Rev. D* **64**, 042004 (2001).
- [28] B. Allen, W. G. Anderson, P. R. Brady, D. A. Brown, and J. D. E. Creighton, *Phys. Rev. D* **85**, 122006 (2012).
- [29] L. S. Finn, *Phys. Rev. D* **46**, 5236 (1992).
- [30] L. S. Finn and D. F. Chernoff, *Phys. Rev. D* **47**, 2198 (1993).
- [31] B. P. Abbott *et al.*, *Classical and Quantum Gravity* **33**, 134001 (2016).
- [32] L. K. Nuttall, T. J. Massinger, J. Areeda, J. Betzwieser, S. Dwyer, *et al.*, *Classical and Quantum Gravity* **32**, 245005 (2015).
- [33] C. Messick, K. Blackburn, P. Brady, P. Brockill, K. Cannon, *et al.*, *Phys. Rev. D* **95**, 042001 (2017).
- [34] B. P. Abbott *et al.* (LIGO Scientific Collaboration and Virgo Collaboration), *Phys. Rev. X* **6**, 041015 (2016).
- [35] B. P. Abbott *et al.* (LIGO Scientific Collaboration and Virgo Collaboration), *Phys. Rev. D* **96**, 022001 (2017).
- [36] B. P. Abbott *et al.* (LIGO Scientific Collaboration and Virgo Collaboration), *Phys. Rev. D* **93**, 122003 (2016).
- [37] B. P. Abbott *et al.* (LIGO Scientific Collaboration and Virgo Collaboration), *Phys. Rev. X* **6**, 041015 (2016).
- [38] A. H. Nitz, T. Dent, G. S. Davies, S. Kumar, C. D. Capano, *et al.*, *The Astrophysical Journal* **891**, 123 (2020).
- [39] H. Gabbard, M. Williams, F. Hayes, and C. Messenger, *Phys. Rev. Lett.* **120**, 141103 (2018).
- [40] M. B. Schäfer, F. Ohme, and A. H. Nitz, *Phys. Rev. D* **102**, 063015 (2020).
- [41] E. Cuoco, J. Powell, M. Cavaglià, K. Ackley, M. Bejger, *et al.*, “Enhancing gravitational-wave science with machine learning,” (2020), [arXiv:2005.03745](https://arxiv.org/abs/2005.03745) [astro-ph.HE].
- [42] S. R. Green, C. Simpson, and J. Gair, “Gravitational-wave parameter estimation with autoregressive neural network flows,” (2020), [arXiv:2002.07656](https://arxiv.org/abs/2002.07656) [astro-ph.IM].
- [43] D. George and E. A. Huerta, *Phys. Rev. D* **97**, 044039 (2018).
- [44] D. George and E. Huerta, *Physics Letters B* **778**, 64 (2018).
- [45] M. L. Chan, I. S. Heng, and C. Messenger, *Phys. Rev. D* **102**, 043022 (2020).
- [46] S. Coughlin, S. Bahaadini, N. Rohani, M. Zevin, O. Patane, *et al.*, *Phys. Rev. D* **99**, 082002 (2019).
- [47] C. Szegedy, V. Vanhoucke, S. Ioffe, J. Shlens, and Z. Wojna, in *Proceedings of the IEEE conference on computer vision and pattern recognition* (2016) pp. 2818–2826.
- [48] A. H. Nitz, T. Dent, T. D. Canton, S. Fairhurst, and D. A. Brown, *The Astrophysical Journal* **849**, 118 (2017).
- [49] T. Venumadhav, B. Zackay, J. Roulet, L. Dai, and M. Zaldarriaga, *Phys. Rev. D* **100**, 023011 (2019).
- [50] B. Zackay, T. Venumadhav, L. Dai, J. Roulet, and M. Zaldarriaga, *Phys. Rev. D* **100**, 023007 (2019).
- [51] M. Manteiga, I. Carricajo, A. Rodríguez, C. Dafonte, and B. Arcay, *The Astronomical Journal* **137**, 3245 (2009).
- [52] J. S. Almeida and C. A. Prieto, *The Astrophysical Journal* **763**, 50 (2013).
- [53] T. Kuntzer, M. Tewes, and F. Courbin, *Astron. & Astrophys.* **591**, A54 (2016), [arXiv:1605.03201](https://arxiv.org/abs/1605.03201) [astro-ph.IM].
- [54] S. Abraham, N. Mukund, A. Vibhute, V. Sharma, S. Iyyani, *et al.*, “A machine learning approach for grb detection in astrosat czti data,” (2020), [arXiv:1906.09670](https://arxiv.org/abs/1906.09670) [astro-ph.IM].
- [55] N. S. Philip, Y. Wadadekar, A. Kembhavi, and K. B. Joseph, *Astron. & Astrophys.* **385**, 1119 (2002), [arXiv:astro-ph/0202127](https://arxiv.org/abs/astro-ph/0202127) [astro-ph].

- [56] S. C. Odewahn, S. H. Cohen, R. A. Windhorst, and N. S. Philip, *Astrophys. J.* **568**, 539 (2002), [arXiv:astro-ph/0110275](https://arxiv.org/abs/astro-ph/0110275) [astro-ph].
- [57] X. Li, Y. Lin, and K. Qiu, arXiv e-prints, arXiv:1903.07939 (2019), [arXiv:1903.07939](https://arxiv.org/abs/1903.07939) [astro-ph.IM].
- [58] G. T. Richards, A. D. Myers, A. G. Gray, R. N. Riegel, R. C. Nichol, *et al.*, *The Astrophysical Journal Supplement Series* **180**, 67 (2008).
- [59] S. Abraham, N. S. Philip, A. Kembhavi, Y. G. Wadadekar, and R. Sinha, *Mon. Not. R. Astron. Soc.* **419**, 80 (2012).
- [60] C. M. Peters *et al.*, *The Astrophysical Journal* **811**, 95 (2015).
- [61] N. Mukund, S. Abraham, S. Kandhasamy, S. Mitra, and N. S. Philip, *Phys. Rev. D* **95**, 104059 (2017).
- [62] J. Deng, W. Dong, R. Socher, L.-J. Li, K. Li, and L. Fei-Fei, in *2009 IEEE conference on computer vision and pattern recognition* (Ieee, 2009) pp. 248–255.
- [63] A. Krizhevsky, I. Sutskever, and G. E. Hinton, in *Advances in neural information processing systems* (2012) pp. 1097–1105.
- [64] K. He, X. Zhang, S. Ren, and J. Sun, in *Proceedings of the IEEE conference on computer vision and pattern recognition* (2016) pp. 770–778.
- [65] C. Szegedy, W. Liu, Y. Jia, P. Sermanet, S. Reed, *et al.*, in *Proceedings of the IEEE conference on computer vision and pattern recognition* (2015) pp. 1–9.
- [66] J. D. Creighton and W. G. Anderson, *Gravitational-wave physics and astronomy: An introduction to theory, experiment and data analysis* (John Wiley & Sons, 2012).
- [67] B. Allen, *Phys. Rev. D* **71**, 062001 (2005).
- [68] M. Zevin, S. Coughlin, S. Bahaadini, E. Besler, N. Rohani, *et al.*, *Classical and Quantum Gravity* **34**, 064003 (2017).
- [69] L. Debnath and F. A. Shah, *Wavelet transforms and their applications* (Springer, 2002).
- [70] S. Bahaadini, V. Noroozi, N. Rohani, S. Coughlin, M. Zevin, J. Smith, V. Kalogera, and A. Katsaggelos, *Information Sciences* **444**, 172 (2018).
- [71] N. Qian, *Neural Networks* **12**, 145 (1999).
- [72] A. H. Nitz, *Classical and Quantum Gravity* **35**, 035016 (2018).
- [73] “MLStat search data release,” <https://github.com/shreejit-92/MLStat-1.git>.
- [74] T. D. Canton and I. W. Harry, “Designing a template bank to observe compact binary coalescences in advanced ligo’s second observing run,” (2017), [arXiv:1705.01845](https://arxiv.org/abs/1705.01845) [gr-qc].
- [75] G. Ashton and E. Thrane, *Monthly Notices of the Royal Astronomical Society* **498**, 1905 (2020), <https://academic.oup.com/mnras/article-pdf/498/2/1905/33752535/staa2332.pdf>.
- [76] G. Pratten and A. Vecchio, “Assessing gravitational-wave binary black hole candidates with bayesian odds,” (2020), [arXiv:2008.00509](https://arxiv.org/abs/2008.00509) [gr-qc].
- [77] Y. Huang, C.-J. Haster, S. Vitale, A. Zimmerman, J. Roulet, T. Venumadhav, B. Zackay, L. Dai, and M. Zaldarriaga, “Source properties of the lowest signal-to-noise-ratio binary black hole detections,” (2020), [arXiv:2003.04513](https://arxiv.org/abs/2003.04513) [gr-qc].
- [78] G. Ashton *et al.*, *Astrophys. J. Suppl.* **241**, 27 (2019), [arXiv:1811.02042](https://arxiv.org/abs/1811.02042) [astro-ph.IM].
- [79] I. M. Romero-Shaw, C. Talbot, S. Biscoveanu, V. D’Emilio, G. Ashton, *et al.*, *Monthly Notices of the Royal Astronomical Society* (2020), 10.1093/mnras/staa2850, <https://academic.oup.com/mnras/advance-article-pdf/doi/10.1093/mnras/staa2850/33777524/staa2850.pdf>.
- [80] Bécsy, Bence and Raffai, Peter and Cornish, Neil J. and Essick, Reed and Kanner, Jonah and others, *Astrophys. J.* **839**, 15 (2017), [arXiv:1612.02003](https://arxiv.org/abs/1612.02003) [astro-ph.HE].
- [81] R. Cotesta, S. Marsat, and M. Pürrer, *Phys. Rev. D* **101**, 124040 (2020), [arXiv:2003.12079](https://arxiv.org/abs/2003.12079) [gr-qc].
- [82] C. Hoy and V. Raymond, (2020), [arXiv:2006.06639](https://arxiv.org/abs/2006.06639) [astro-ph.IM].